Numerical predictions for laminar source–sink flow in a rotating cylindrical cavity

By J. W. CHEW†, J. M. OWEN AND J. R. PINCOMBE

School of Engineering and Applied Sciences, University of Sussex, Falmer, Brighton, England

Numerical solutions are presented for steady, axisymmetric, laminar, isothermal, source–sink flow in a rotating cylindrical cavity. These results, which are in good agreement with previously published experimental work, have been used to give a fresh insight into the nature of the flow and to investigate the validity of other theoretical solutions. When the fluid enters the cavity through a central uniform radial source and leaves through an outer sink, it is shown that the flow near the disks can be approximated by two known analytical solutions. If the radial source is replaced by an axial inlet the flow becomes more complex, with a wall jet forming on the downstream disk at sufficiently high flow rates.

1. Introduction

A rotating cylindrical cavity with a radial outflow of fluid provides a simple model of the flow between corotating gas-turbine disks. In the turbine, cooling air usually enters axially, through a central hole of radius $r = a$ in one disk, and leaves radially through a series of holes in a peripheral cylindrical shroud at $r = b$. Although the flow in such systems is almost invariably turbulent and non-isothermal, the study of laminar isothermal flow can throw considerable light on the problem.

Insight into the structure of laminar source–sink flow inside a rotating cavity has been provided by Hide (1968). For isothermal radial outflow from a uniform source at $r = a$ to a uniform sink at $r = b$, the flow can be divided into four regions: an inner source region (which, for some flows, may be so large that the commonly used expression 'source layer' seems inappropriate); separate Ekman layers on each disk; an outer sink layer; and an interior inviscid core which is bounded by the abovenamed layers. Hide obtained analytical solutions for the velocity distribution in the four regions by matching the linear Ekman-layer solution to boundary-layer solutions on the source and sink; he also provided estimates for the radial extent of the source region and the sink layer.

The accuracy of Hide's solutions has been investigated by Bennetts & Hocking (1973), who computed a nonlinear Ekman-layer solution, and by Bennetts & Jackson (1974), who obtained numerical solutions of the Navier–Stokes equations. When the volumetric flow rate Q is relatively small, Hide's linear solution gives a good representation of the flow; as the flow rate is increased, the linear solution becomes increasingly less accurate.

Owen & Pincombe (1980) used flow visualization and laser-Doppler anemometry to determine the flow structure and to measure the velocity distribution inside an isothermal rotating cavity with radial outflow. Air was admitted to the centre of the cavity either axially or radially (through a gauze screen), and the flow left the cavity

† Present address: Theoretical Science Group, Rolls-Royce Limited, P.O. Box 31, Derby, England.

through a series of holes in the shroud. For the radial inlet case, the flow structure was qualitatively (and, for the lower flow rates, it was quantitatively) similar to that determined by Hide. The nature and size of the source region was found to depend on whether the flow entered axially or radially; in the former case, a wall jet could form on the downstream disk, and the radial extent of the source region was greater than that of the radial inlet case. For the latter case, the extent of the source region was found to be in good agreement with an expression giving the radius at which Faller's (1963) nonlinear Ekman solution gave zero rotation in the core.

Heat-transfer measurements were made in rotating cavities by Owen & Bilimoria (1977) and by Owen & Onur (1983). For the radial-outflow case (where air entered the cavity axially, and the downstream disk was heated), a number of turbulent heat-transfer regimes were delineated. In regime I, at relatively low rotational speeds, the heat transfer was found to be independent of rotational speed; at higher speeds, in regime II, the heat transfer increased with both increasing flow rate and increasing speed; regimes III and IV occurred at even higher rotational speeds where, particularly in regime IV, buoyancy forces were significant.

For non-isothermal laminar and turbulent flow, Owen & Rogers (1983) derived integral equations for flow inside an Ekman layer in a rotating cavity with source–sink flow; approximate solutions were obtained for the linear equations. Rogers & Owen (1983) obtained numerical solutions of the nonlinear integral equations; these solutions were shown to be in good agreement with a large range of experimental data, for laminar and turbulent source–sink flows, by Pincombe, Owen & Rogers (1983). It is worth noting that the criterion, suggested by these authors, for transition from laminar to turbulent flow in an Ekman layer is $Re_r \approx 180$ (where $Re_r = Q/vr$, v being the kinematic viscosity of the fluid).

In this paper, numerical solutions of the Navier–Stokes equations are presented for the case of axisymmetric isothermal laminar flow in a rotating cavity with a radial outflow. These solutions, which were obtained using the method of Chew (1984), provide an essential step towards the ultimate objective of obtaining numerical solutions for non-isothermal turbulent flow in a rotating cavity. The solutions are compared with the data of Owen & Pincombe and with the analytical results of other authors. Section 2 outlines the numerical method and the boundary conditions used, and the numerical solutions for the rotating cavity with a radial inlet and with an axial inlet are discussed in §§3 and 4 respectively.

2. An outline of the numerical method

Full details of the numerical method are given by Chew (1984). In this reference, the techniques employed here were shown to give excellent agreement with Hide's (1968) analytical solution in the linear flow regime. For completeness, an outline of the method, and details of the boundary conditions are presented below.

For steady axisymmetric laminar flow, with density ρ and constant viscosity μ, the Navier–Stokes and continuity equations can be expressed as

$$\frac{1}{r}\frac{\partial(\rho r u^2)}{\partial r}+\frac{\partial(\rho u w)}{\partial z}=-\frac{\partial p'}{\partial r}+\mu\left[\frac{1}{r}\frac{\partial}{\partial r}\left(r\frac{\partial u}{\partial r}\right)+\frac{\partial^2 u}{\partial z^2}-\frac{u}{r^2}\right]+2\rho\Omega v+\frac{\rho v^2}{r},$$

(2.1)

$$\frac{1}{r}\frac{\partial(\rho r u v)}{\partial r}+\frac{\partial(\rho v w)}{\partial z}=\mu\left[\frac{1}{r}\frac{\partial}{\partial r}\left(r\frac{\partial v}{\partial r}\right)+\frac{\partial^2 v}{\partial z^2}-\frac{v}{r^2}\right]-\frac{\rho u v}{r}-2\rho\Omega u,$$

(2.2)

$$\frac{1}{r}\frac{\partial(\rho r u w)}{\partial r}+\frac{\partial(\rho w^2)}{\partial z}=-\frac{\partial p'}{\partial z}+\mu\left[\frac{1}{r}\frac{\partial}{\partial r}\left(r\frac{\partial w}{\partial r}\right)+\frac{\partial^2 w}{\partial z^2}\right], \tag{2.3}$$

$$\frac{1}{r}\frac{\partial(ru)}{\partial r}+\frac{\partial w}{\partial z}=0, \tag{2.4}$$

where u, v, w are the velocity components relative to the cylindrical coordinate system r, θ, z (rotating at angular speed Ω about $r = 0$). The static pressure p is related to the reduced pressure p' by

$$p' = p - \tfrac{1}{2}\rho\Omega^2 r^2. \tag{2.5}$$

Solutions were obtained for the experimental conditions of Owen & Pincombe (1980). For the cylindrical cavity, $a = 19$ mm, $b = 190$ mm and $s = 50.7$ mm (the axial width between the two disks); for the air, $\rho = 1.225$ kg m^{-3} and $\mu = 1.78 \times 10^{-5}$ kg m^{-1} s^{-1}.

For the radial inlet tests, the following boundary conditions were used:

$$u = \frac{Q}{2\pi r s} \quad \text{and} \quad v = w = 0 \quad \text{at} \quad r = a, b, \tag{2.6}$$

$$u = v = w = 0 \quad \text{at} \quad z = 0, \tag{2.7}$$

$$\frac{\partial u}{\partial z} = \frac{\partial v}{\partial z} = w = 0 \quad \text{at} \quad z = \tfrac{1}{2}s, \tag{2.8}$$

For the axial inlet tests:

$$u = \frac{\partial v}{\partial r} = \frac{\partial w}{\partial r} = 0 \quad \text{at} \quad r = 0, \tag{2.9}$$

$$u = \frac{Q}{2\pi b s} \quad \text{and} \quad v = w = 0 \quad \text{at} \quad r = b, \tag{2.10}$$

$$u = v = 0 \quad \text{and} \quad w = \frac{Q}{\pi a_c^2} \quad \text{at} \quad z = 0, \quad 0 < r < a_c, \tag{2.11}$$

$$u = v = w = 0 \quad \text{at} \quad z = 0, \quad a_c < r < b, \tag{2.12}$$

$$u = v = w = 0 \quad \text{at} \quad z = s, \quad 0 < r < b. \tag{2.13}$$

The axial-inlet radius a_c used in the computations was chosen to be midway between two grid points; in the finite-difference grid used, this meant that $a_c = 20.2$ mm compared with $a = 19$ mm in the experiments.

The above equations were converted to finite-difference form and were solved by a modified version of the TEACH program (Gosman & Ideriah 1976). One modification, made by Chew (1984), introduced step changes in grid size, so as to economize on the total number of grid points required, while still obtaining sufficient resolution in the boundary layers. Another modification used 'Aitken's extrapolation' to accelerate the solution of the finite-difference equations.

For the radial-inlet case, most runs were carried out with a non-uniform finite-difference grid with 32 axial and 44 radial locations; a number of results were repeated with different grids to ensure that truncation errors were not significant. For the axial-inlet case, it was found that a non-uniform grid with 45 axial lines and 43 radial locations were sufficient to reduce truncation errors to insignificant levels. The computation was carried out on the University of Manchester's CDC 7600 computer; typically between 10 and 20 min of CPU time was required.

To aid interpretation of the numerical results, values of the axisymmetric stream

function were calculated from the velocity solutions, and streamline patterns were then produced using a standard contour package. As the plotting program interpolated from the finite-difference grid onto a coarser contour-plotting mesh, before interpolating from this grid to get the streamline paths, some distortion of the results in this process is inevitable. Although these plots do not give a completely accurate representation of the flow, they do give a useful overall picture and provide insight into the flow structure.

3. The radial-inlet case

It is convenient to introduce a dimensionless flow rate C_w, a rotational Reynolds number Re_θ and a Rossby number ϵ_r, where

$$C_w = Q/\nu b, \tag{3.1}$$

$$Re_\theta = \Omega b^2/\nu \tag{3.2}$$

and

$$\epsilon_r = b^2 C_w/4\pi r^2 Re_\theta^{\frac{1}{2}}. \tag{3.3}$$

3.1. *Comparison with experimental results*

Figure 1 shows a comparison of streamline plots obtained from the numerical results and the smoke pattern photographed by Owen & Pincombe (1980) for $Re_\theta = 2.5 \times 10^4$ and $C_w = 79$. Note that the flow visualization photograph (*b*) shows reflections at the surface of the two perspex disks; these should be ignored as they do not form part of the flow. This figure shows good agreement between prediction and experiment with the size of the different flow regions corresponding almost exactly.

Numerical solutions were also obtained for the same value of Re_θ at the higher flow rates corresponding to $C_w = 192$, 331 and 605. The main effect of increasing C_w on the predicted flow structure shown in figure 1 (*a*) was an increase in the radial extent of the source region. Not surprisingly, the numerical method (which is, of course, limited to the steady axisymmetric case) did not predict either the flow instabilities within the source region or the cellular structure of the Ekman layers observed experimentally at the higher flow rates.

Figure 2 shows a comparison of the numerical predictions with Owen & Pincombe's measurements for the radial and tangential components of velocity (obtained using laser-Doppler anemometry). Here the radial velocity has been non-dimensionalized with division by the inlet velocity $U = Q/2\pi as$. Again, the results from the computer model are in good agreement with experiment. Owen & Pincombe also measured the extent of the source region, but discussion of this is deferred to §3.2.

3.2. *Comparison with analytical results*

For the Ekman layers, (2.1)–(2.4) can be truncated to boundary-layer form; and, for small values of the Rossby number, the nonlinear terms can be neglected. The resulting solution of the linear Ekman-layer equations is

$$\left. \begin{array}{l} \dfrac{u}{\Omega r} = 2\epsilon_r(e^{-\xi}\sin\xi + e^{-\xi^*}\sin\xi^*), \\[2mm] \dfrac{v}{\Omega r} = -2\epsilon_r(1 - e^{-\xi}\cos\xi - e^{-\xi^*}\cos\xi^*), \\[2mm] w = 0, \\[2mm] \xi = z\left(\dfrac{\Omega}{\nu}\right)^{\frac{1}{2}}, \quad \xi^* = (s-z)\left(\dfrac{\Omega}{\nu}\right)^{\frac{1}{2}}. \end{array} \right\} \tag{3.4}$$
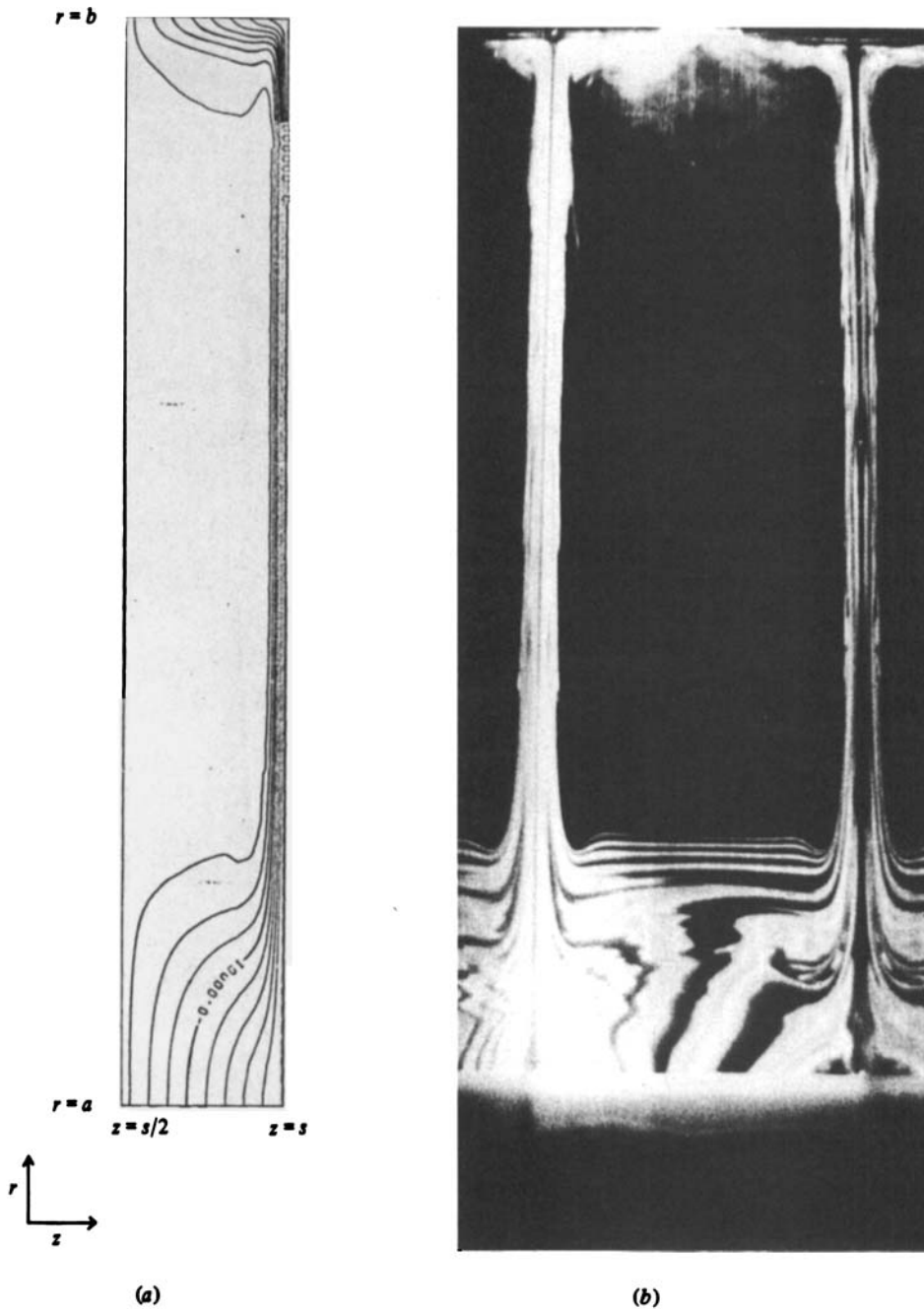
where

FIGURE 1. Flow structure, for the case of a radial inlet, for $Re_\theta = 2.5 \times 10^4$ and $C_w = 79$: (a) streamlines in the (r, z)-plane predicted by the numerical method for the half-cavity $\frac{1}{2}s \leqslant z \leqslant s$; (b) smoke patterns photographed by Owen & Pincombe (1980).

Comparisons between the computed velocities and Hide's (1968) solution (which modifies (3.4) in the source region and in the sink layer) for $Re_\theta = 2.5 \times 10^4$ and $C_w = 192$ are shown in figure 3. As was found by Bennetts & Jackson (1974), the numerical results depart from Hide's solutions as the flow rate is increased. In particular, there is a significant difference between the analytical and numerical solutions in the source region. It should be noted that Hide assumed a thin boundary
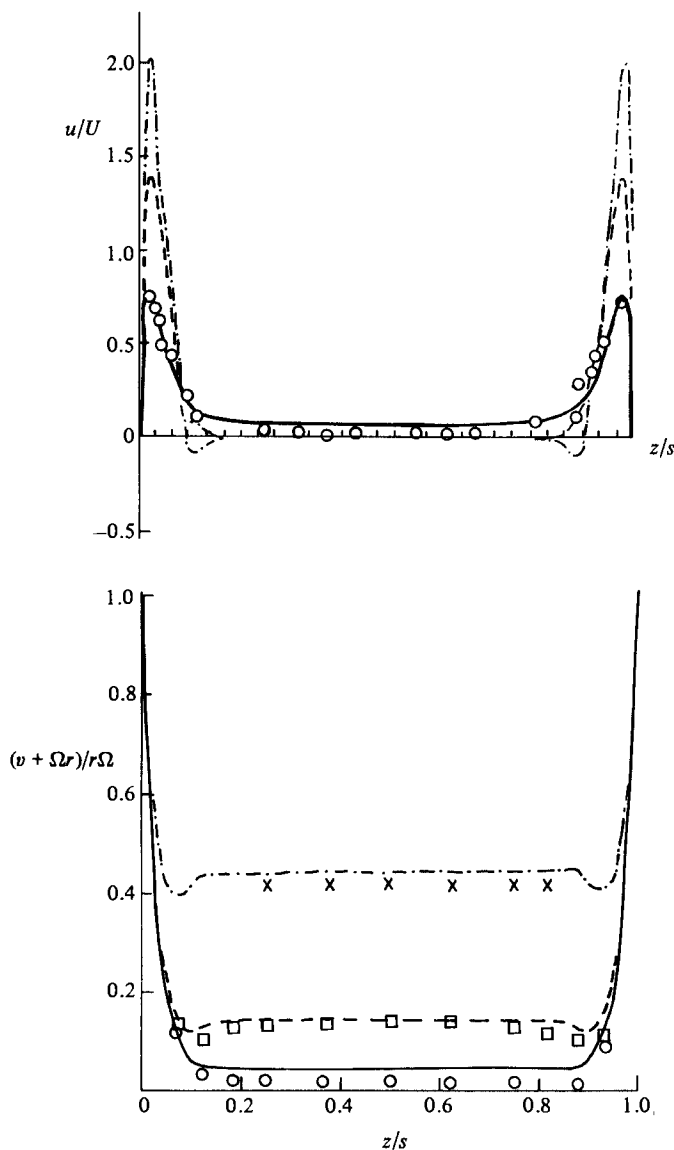
FIGURE 2. Axial distribution of radial and tangential components of velocity, for the case of a radial inlet, for $Re_\theta = 2.5 \times 10^4$ and $r/a = 6.0$.

Flow rate C_w	192	331	605
Numerical solutions	—·—·—	―――	――――
Owen & Pincombe (1980)	×	□	○

layer on $r = a$ (which is obviously not the case in figure 3); he also did not use the no-slip conditions for w at $r = a$ and $r = b$.

Also shown in figure 3(*b*) is Faller's (1963) nonlinear solution (truncated to second order in ϵ_r) for the tangential velocity in the core and Rogers & Owen's (1983) nonlinear integral momentum solution. The latter solutions were computed assuming $v = 0$ at $r = a$, whereas Faller's solution is independent of inlet conditions. Neither of these methods takes account of the conditions at $r = b$, so these solutions cannot be expected to be valid in the sink layer. It can be seen that the Rogers & Owen
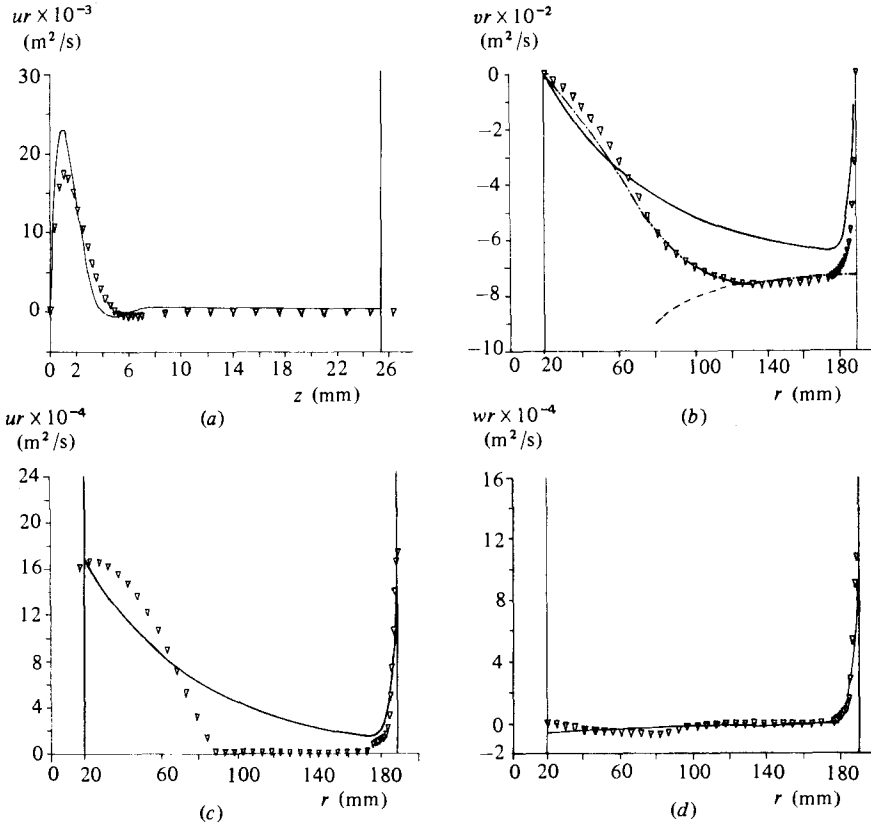
FIGURE 3. Radial and axial distributions of velocity, for the case of a radial inlet, for $Re_\theta = 2.5 \times 10^4$ and $C_w = 192$: (a) axial distribution of ur at $r = 104$ mm; (b) radial distribution of vr at $z = 26$ mm; (c) radial distribution of ur at $z = 26$ mm; (d) radial distribution of wr at $z = 4$ mm. ∇, Numerical solutions; ——, Hide (1968); - - - - -, Faller (1963); —·—, Rogers & Owen (1983).

solution is in reasonable agreement with the numerical results throughout the source region and is in good agreement in the core region. Note that in the source region Faller's solution implies that the fluid rotates in the opposite direction to the disk. This clearly contradicts the experimental and numerical results, which show that the fluid always rotates in the same sense as the disk, for these inlet conditions.

In their experimental work, Owen & Pincombe estimated the radial extent of the source region from the flow-visualization results. They found that, for the radial-inlet case, the experimentally observed outer radius of the source region concurred with the point at which Faller's solution for the tangential velocity in the core became zero (in a stationary frame of reference). Denoting the edge of the source region by $r = r_s$, Owen & Pincombe's results may be written

$$\frac{r_s}{a} = 0.423\frac{b}{a}C_w^{\frac{1}{2}}Re_\theta^{-\frac{1}{4}}. \tag{3.5}$$

Table 1 shows a comparison, for $Re_\theta = 2.5 \times 10^4$, between the extent of the source region $(r_s - a)$ calculated from (3.5) and the '90% thickness', calculated from Hide's solution and from the numerical results. Here, the '90% thickness' is defined by the radius at which ru, in the midaxial plane, equals 10% of the value at $r = a$; the radial velocity being preferred to the tangential velocity in this definition, as it is the former

Mass-flow parameter C_w	Source: $r_s - a$			Sink	
	90% thickness: numerical results	90% thickness: Hide's theory	Equation (3.5)	90% thickness: numerical results	90% thickness: Hide's theory
0.01	14.9	12.7	—	12.2	12.7
79	35.8	60.6	37.8	9.7	10.1
192	63.8	142	69.6	7.3	7.5
331	88.6	243	97.3	5.0	5.4
605	125.5	—	138.2	3.8	3.4

TABLE 1. The thickness (mm) of the source region and the sink layer for radial outflow with radial inlet, $Re_\theta = 2.5 \times 10^4$

that controlled the advection of smoke into the cavity in the experiments. It can be seen that Hide's theory overestimates the thickness of the source region at the higher values of C_w, whereas the numerical results for the '90% thickness' are lower than those given by (3.5), but follow similar trends, as might be expected. Also included in table 1 are the numerical estimates of the '90% thickness' of the sink layer; these are consistent with the values obtained from Hide's theory.

Some insight into the flow structure within the source region can be gained by examining the development of the disk boundary layer. In figure 4 the computed radial velocity profiles across this layer are shown at several radial positions for $Re_\theta = 2.5 \times 10^4$ and $C_w = 79$ and 605. Here the velocities are normalized with respect to Ωr and the non-dimensional variable ξ is used for the axial coordinate. Also shown in this figure is the linear Ekman solution (3.4) and von Kármán's (1921) solution for the so-called free disk (an infinite disk rotating in a quiescent environment) as computed by Cochran (1934). It can be seen that for $C_w = 79$ the numerical results are close to the free-disk solution at the smaller values of r/a and agree with the Ekman solution at the larger values of r/a. For $C_w = 605$ the solution appears to develop towards that of the free disk as the radius increases.

It should be noted that within the source region, away from the boundary layers, the angular momentum of the fluid can be expected to be conserved as the fluid moves radially outwards; thus $v + \Omega r \propto 1/r$ in this region. Also, towards the outer limit of the source region, the radial velocity away from the boundary layer will be much less than that within the entraining boundary layer, owing to the different axial length-scales in these regions. From these considerations it follows that, in considering the boundary layer, the values of u and v towards the outer limit of the source region may be approximated, respectively, by 0 and $-\Omega r$ at the edge of the boundary layer. As these are exactly the conditions satisfied by von Kármán's solution, the behaviour of the numerical results in figure 4 is not surprising.

From the above argument and from the numerical results, it follows that, towards the outer part of the source region, the radial flow rate in the disk boundary layer is approximately equal to that in von Kármán's free-disk problem, which from Cochran's solution is given by

$$Q_e = 0.886\pi r^2 (\nu\Omega)^{\frac{1}{2}}. \tag{3.6}$$

Note that, although u is assumed to be negligible outside the boundary layer in deriving this result, the total radial flow of fluid in the inviscid region may still be significant owing to the different axial lengthscales between the two regions. Away from the boundary layers, the total radial flow rate is assumed to be zero at the outer
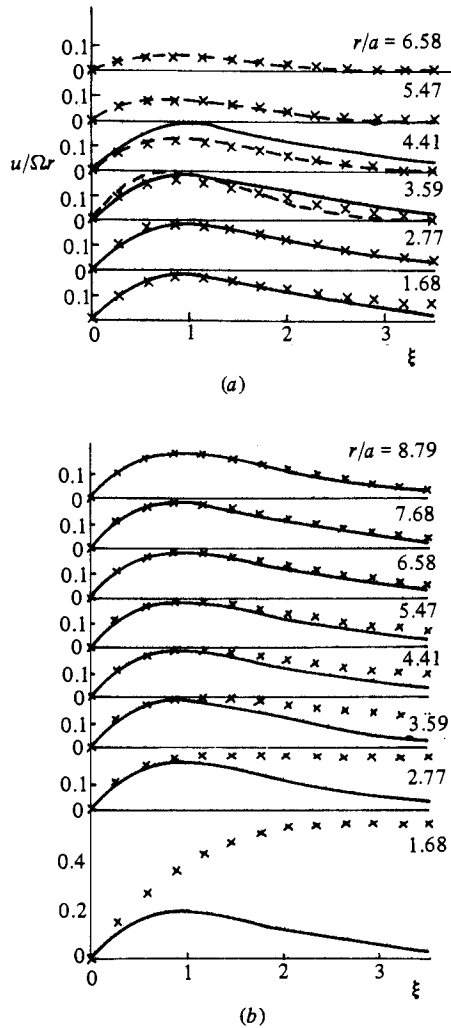
FIGURE 4. Axial distribution of radial component of velocity, for the case of a radial inlet, for $Re_\theta = 2.5 \times 10^4$: (a) $C_w = 79$; (b) $C_w = 605$. ×, numerical solutions; ----, Ekman-layer solution; ——, free-disk solution.

edge of the source region; at this point, the flow rate in the boundary layer on each disk must be equal to $\frac{1}{2}Q$. Hence, to estimate the extent of the source region, it is assumed that $Q_e = \frac{1}{2}Q$ at $r = r_s$, giving

$$\frac{r_s}{a} = 0.424 \frac{b}{a} C_w^{\frac{1}{4}} Re_\theta^{-\frac{1}{4}}, \tag{3.7}$$

which agrees (within 0.25 %) with (3.5). The derivation given here is perhaps more satisfactory than that of Owen & Pincombe, since Faller's solution does not correctly predict v at $r = r_s$, as can be seen from figure 3(b).

An interesting feature of the numerical results was that, at the higher values of C_w studied, some recirculation was predicted at the edge of the outer sink layer. This is apparent in figure 5, which shows how the computed axial velocity varies with radius for four different flow rates at $z/s = 0.259$ with $Re_\theta = 2.5 \times 10^4$. Hide's solution,
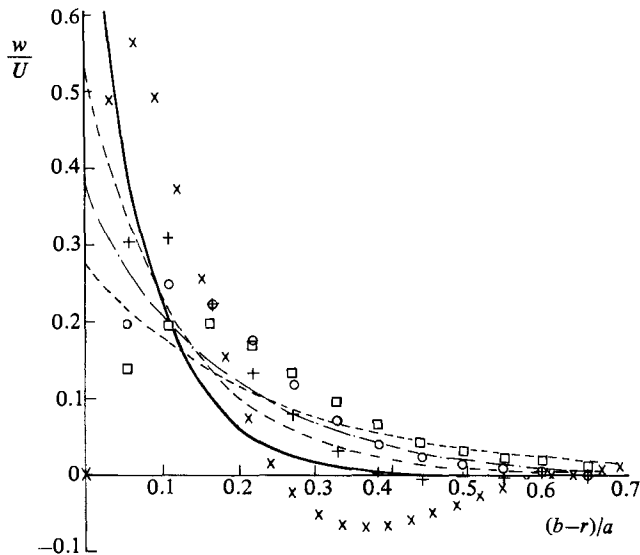
FIGURE 5. Radial distribution of axial component of velocity, for the case of a radial inlet, for $Re_\theta = 2.5 \times 10^4$ and $z/s = 0.259$.

Flow rate C_w	79	192	331	605
Numerical solutions	□	○	+	×
Hide (1968)	-----	—·—·—	———	———

which does not take account of the no-slip condition at $r = b$, is also shown. Of course, without firm experimental evidence it is not possible to say whether or not these numerical results would be realized physically.

4. The axial-inlet case

4.1. *Comparison with experimental results*

Figure 6 shows the comparison between the computed streamlines and the flow visualization for $C_w = 79$ and $Re_\theta = 2.5 \times 10^4$. In the experiments, vortex breakdown was observed under these conditions. The experimental results were non-axisymmetric in the source region, with the central jet precessing about the axis of the cavity, but the flow was axisymmetric outside this region. It is interesting that the numerical method, which assumes a steady axisymmetric result everywhere, has converged to a solution that appears to agree with the experimental observations outside the non-axisymmetric source region.

At higher flow rates or lower rotational speeds, the inlet jet no longer undergoes vortex breakdown, but traverses the cavity and forms a wall jet on the downstream disk. This behaviour is displayed by the streamline plots in figure 7, which show the results for $C_w = 331$ over a range of different Reynolds numbers. The results for the higher values of Re_θ in this figure indicate that the wall jet breaks down owing to the pumping action of the upstream disk, which must entrain half the net flow before the Ekman-layer region is formed. Owen & Pincombe's flow visualization for this class of flow showed an axisymmetric wall jet similar to that predicted here. However, in the region where fluid is discharged from the wall jet, in the source region away from the boundary layers, and in the central jet, their results show non-axisymmetric and
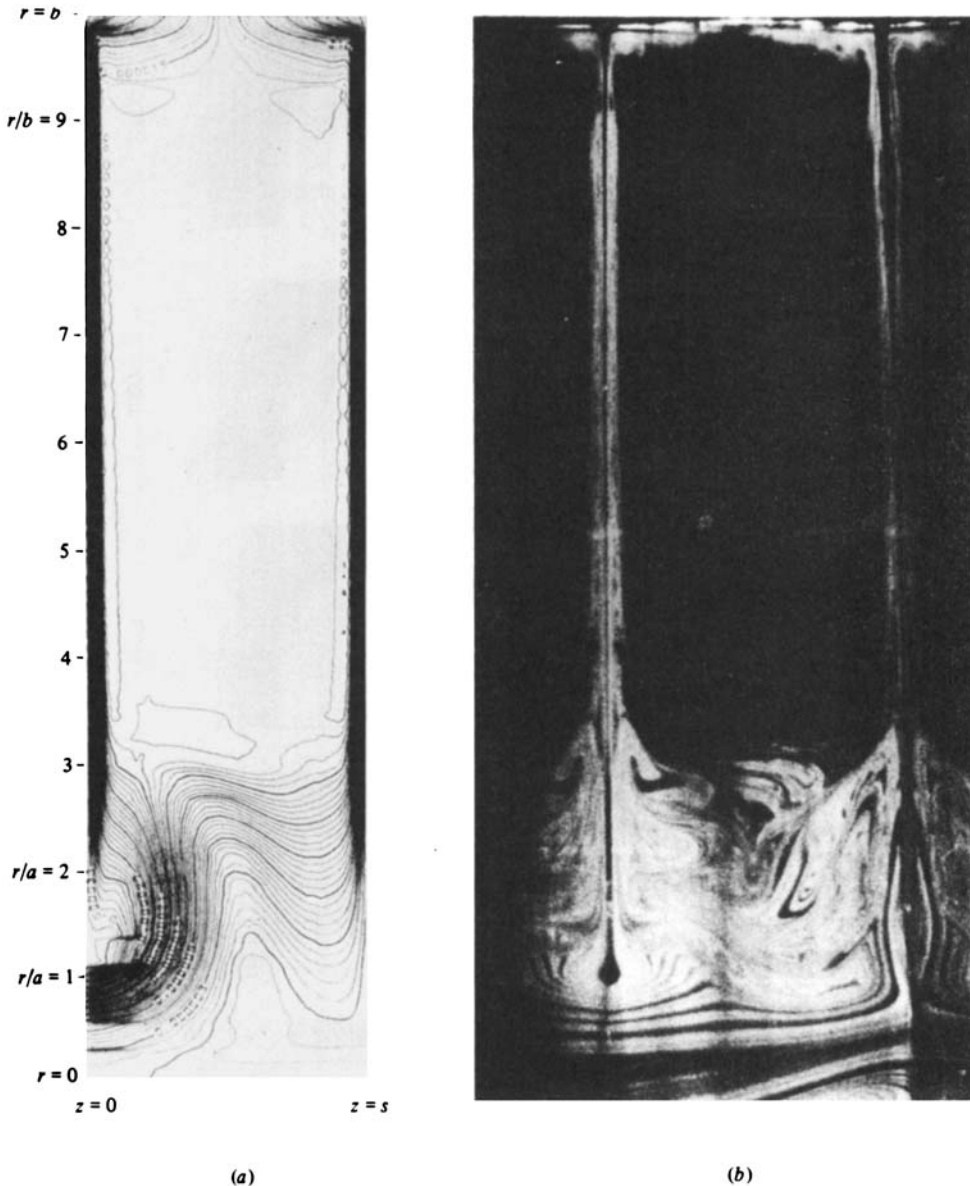
FIGURE 6. Flow structure, for the case of an axial inlet, for $Re_\theta = 2.5 \times 10^4$ and $C_w = 79$: (*a*) streamlines in the (r, z)-plane predicted by the numerical method; (*b*) smoke patterns photographed by Owen & Pincombe (1980).

unsteady flow instabilities. As stated above, these non-axisymmetric effects cannot be predicted by the model used to calculate the results presented in this paper.

The results in figure 7 show qualitatively how transition between the heat-transfer regimes I and II, discussed in §1, may occur. At $Re_\theta = 2 \times 10^3$ the main flow is from the central inlet jet to the wall jet on the downstream disk and then from the wall jet to the sink. As Re_θ increases, rotational effects begin to dominate, and an Ekman-layer region forms towards the outer part of the cavity. Although at higher
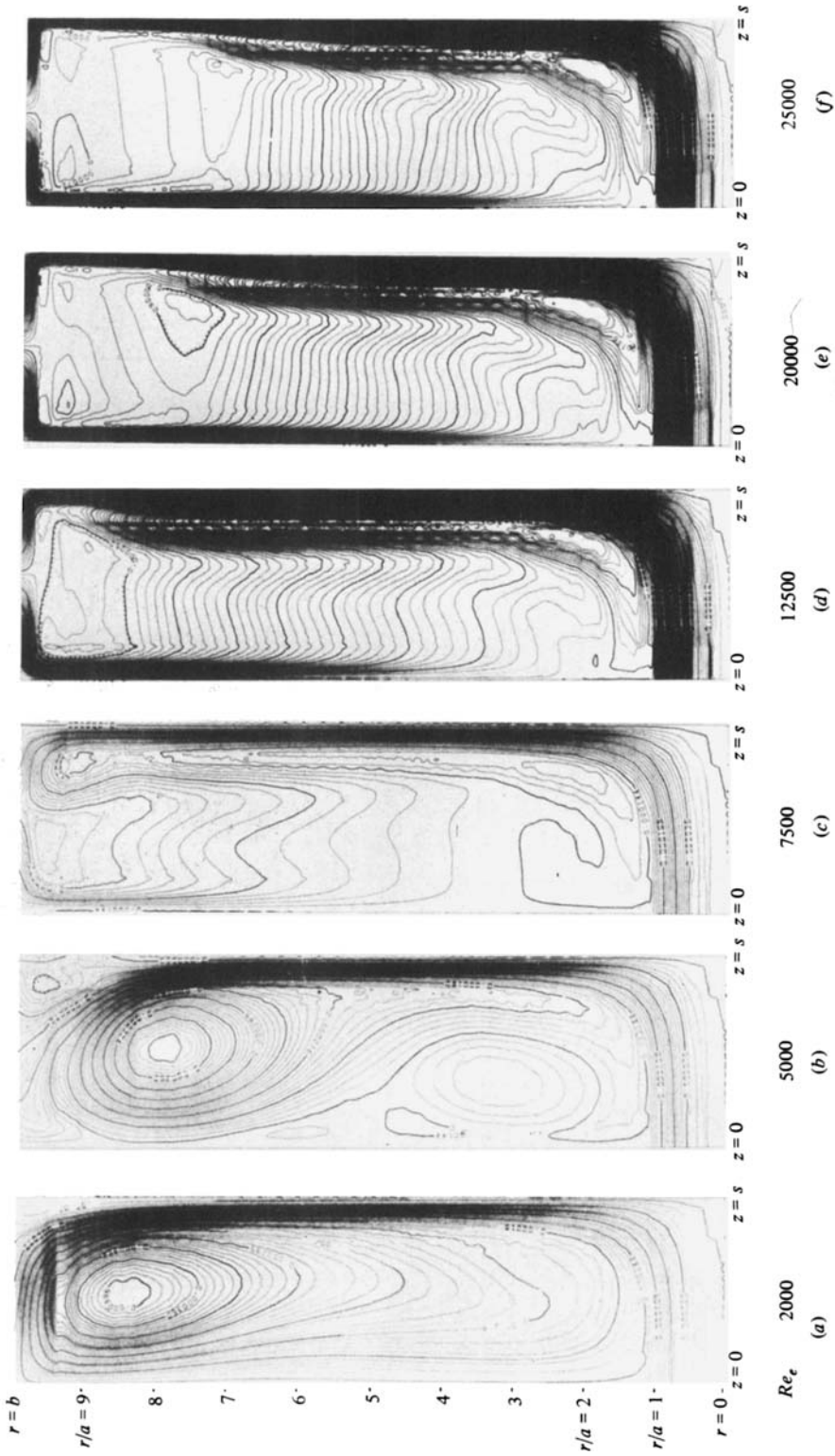
FIGURE 7. Numerically predicted streamlines, for the case of an axial inlet, for $C_w = 331$: (a) $Re_\theta = 2000$; (b) 5000; (c) 7500; (d) 12500; (e) 20000; (f) 25000.
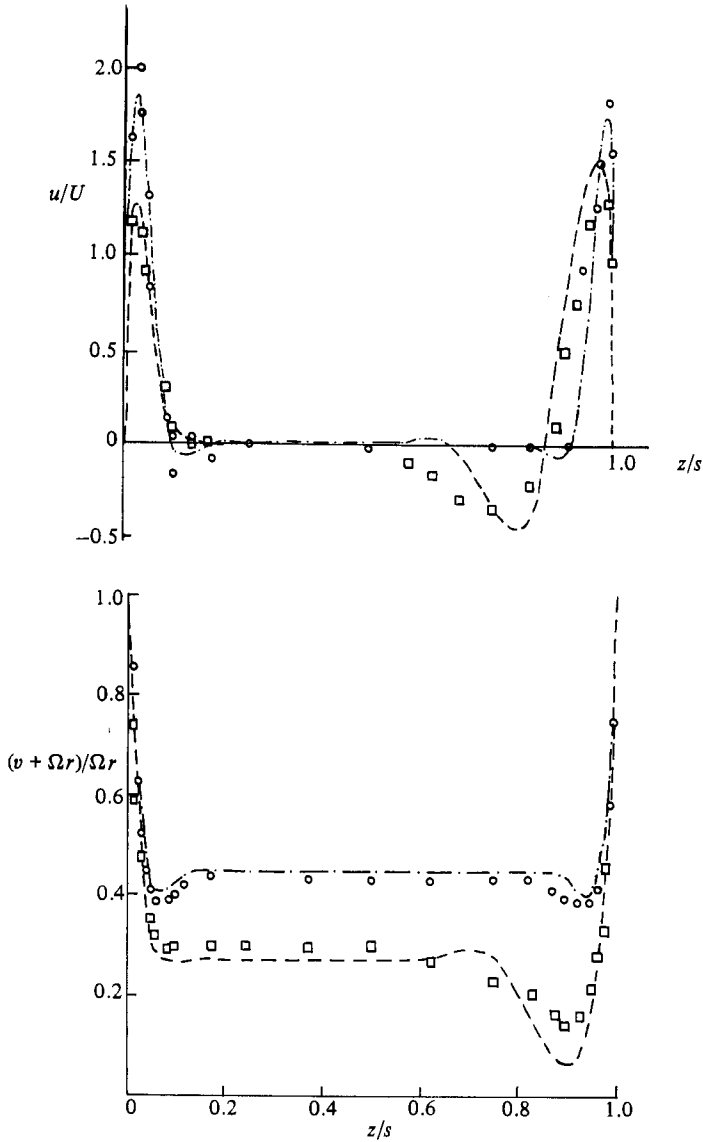
FIGURE 8. Axial distribution of radial and tangential components of velocity, for the case of an axial inlet, for $Re_\theta = 2.5 \times 10^4$ and $r/a = 6.0$.

Flow rate C_w	192	331
Numerical solutions	— · —	- - -
Owen & Pincombe (1980)	○	□

rotational speeds than those shown here the structure of the source region will change, it seems unlikely that this would affect the experimental results (in which the main heat transfer took place in the outer part of the cavity). However, buoyancy forces became more important as Re_θ increases, and so the experimental results can be expected to show effects that do not occur in isothermal flow.

Comparisons between measured and computed radial and tangential velocity components are shown in figure 8 for $Re_\theta = 2.5 \times 10^4$ and $r/a = 6.0$. For $C_w = 192$ this
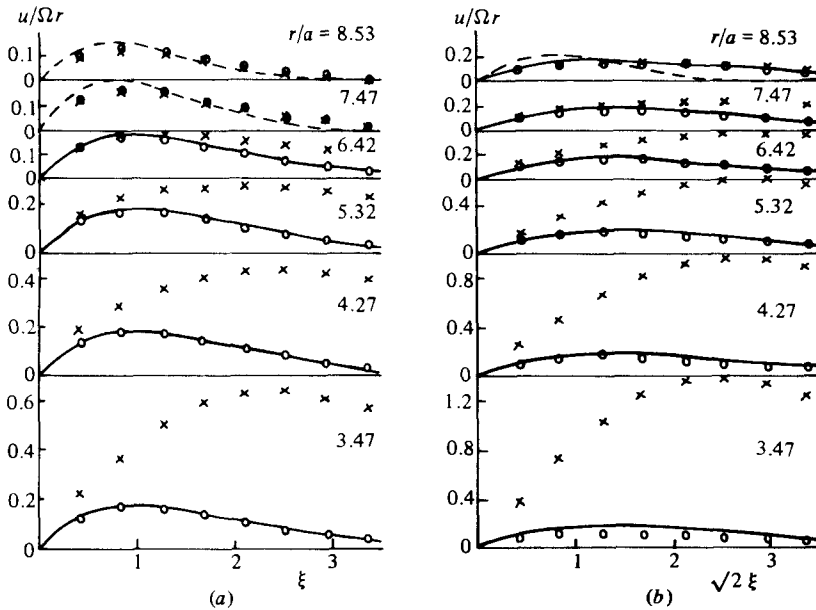
FIGURE 9. Axial distribution of radial component of velocity for the case of an axial inlet, $C_w = 331$:
(a) $Re_\theta = 2.5 \times 10^4$; (b) $Re_\theta = 1.25 \times 10^4$. ×, numerical solution, downstream disk; ○, numerical solution, upstream disk; −−−−, Ekman-layer solution; ——, free-disk solution.

value of r/a is outside the source region, and both the experimental and computed results show that the flow is symmetrical about the midaxial centreline ($z/s = 0.5$). For $C_w = 331$ the radial velocity provides quantification of the features seen in figure 7(f): the boundary layer on the downstream disk (which is inside the source region) is thicker than that on the upstream disk, and a significant amount of reverse flow occurs. The tangential velocity near the downstream disk is significantly lower than that near the upstream disk. Considering the flow instabilities mentioned above, the difference between the numerical and experimental results for $C_w = 331$ near the downstream disk, at $z = s$, is not surprising. Indeed, the similarity between prediction and measurement for this case suggests that the effect of the instabilities is localized, and the mean motion is very similar to that predicted by the numerical solution.

4.2. Comparison with analytical results

The computed values of radial velocity shown in figure 9 give some insight into the flow structure for the axial-inlet case. As for the radial-inlet case of figure 4, the Ekman-layer solution (3.4) and the free-disk solution are shown for comparison, and the non-dimensional axial distance ξ is used for both the upstream and the downstream disks. It should be noted that in figure 9(b) $\sqrt{2}\,\xi$ rather than ξ has been used on the horizontal axis; thus, despite the lower rotational speed, the scaling of this axis to the dimensional distance z is the same in figure 9(b) as it is in figure 9(a).

Looking first at figure 9(a) ($C_w = 331$, $Re_\theta = 2.5 \times 10^4$), the asymmetry between the two disks in the source region ($r/a \leqslant 6.42$) is apparent. The flow close to the downstream disk is considerably greater than that on the upstream disk within this region (owing to the formation of the wall jet noted above). The flow on the upstream disk develops from 'free-disk flow' within the source region to Ekman-layer flow at the larger radii ($r/a \geqslant 7.47$). The explanation for this behaviour is similar to that

given for the radial-inlet case in §3.2: provided that the angular momentum of the fluid discharging from the wall jet is relatively weak, the boundary conditions on the upstream-disk layer will approximate to those of von Kármán's problem. Results at a lower rotational speed ($Re_\theta = 1.25 \times 10^4$) in figure 9(b) show similar behaviour, although Ekman-layer flow does not occur owing to the extension of the source region to $r/a > 8.53$. The results for $r/a \leqslant 4.27$ show that rotational speed only has a small effect on the radial flow in the wall jet; the speed does, of course, affect the extent of the source region.

Examination of the results for the case of $C_w = 79$, $Re_\theta = 2.5 \times 10^4$ (where vortex breakdown occurred experimentally) shown in figure 6 suggests that the disk boundary-layer development in this case is very similar to the radial-inlet case. For $r/a \geqslant 2.7$ the velocity profiles close to the two disks are almost identical, and they coincide with those given in figure 4(a).

5. Conclusions

The computer program described by Chew (1984) has been successfully applied to the study of isothermal laminar source–sink flow in a rotating cavity. The numerical predictions are in good agreement with previously published experimental and analytical results, and have given new insight into the nature of the flow.

For the case of radial outflow with a radial inlet, the manner in which flow is entrained by the disks within the source region is very similar to that of a free disk. As a similarity solution is available for this case, the flow over most of the disks' area can be described, to a fair approximation, in terms of this solution and the Ekman-layer solution.

For radial outflow with an axial inlet, the flow structure of the source region is generally more complex than for a radial inlet. If vortex breakdown occurs, the flow close to the disks is similar to that with a radial inlet; but, if the flow rate is sufficiently high, a wall jet forms on the downstream disk. Although the radial velocities within the wall jet are fairly insensitive to rotational speed, the extent of this region, and consequently the size of the source region, are dependent on the speed. At high rotational speeds the radial component of velocity in the source region near the upstream disk is close to the free-disk value. At sufficiently low rotational speeds, the wall jet extends to the outer edge of the cavity and the flow goes directly from this region to the sink; the flow in the rest of the cavity is then a secondary recirculation.

REFERENCES

BENNETTS, D. A. & HOCKING, L. M. 1973 On nonlinear Ekman and Stewartson layers in a rotating fluid. *Proc. R. Soc. Lond.* A **333**, 469.

BENNETTS, D. A. & JACKSON, W. D. N. 1974 Source–sink flows in a rotating annulus: a combined laboratory and numerical study. *J. Fluid Mech.* **66**, 689.

CHEW, J. W. 1984 Development of a computer program for the prediction of flow in a rotating cavity. *Intl J. Num. Methods Fluids* (to be published).

COCHRAN, W. G. 1934 The flow due to a rotating disc. *Proc. Camb. Phil. Soc.* **30**, 365.

FALLER, A. J. 1963 An experimental study of the instability of the laminar Ekman boundary layer. *J. Fluid Mech.* **15**, 560.

GOSMAN, A. D. & IDERIAH, F. J. K. 1976 TEACH-T: A general computer program for two dimensional turbulent recirculating flows. In *Calculation of Recirculating Flows*. Dept Mech. Engng, Imperial College, University of London.

HIDE, R. 1968 On source–sink flows in a rotating fluid. *J. Fluid Mech.* **32**, 737.

KÁRMÁN, T. VON 1921 Über laminare und turbulente Reibung. *Z. angew. Math. Mech.* **1**, 233.

OWEN, J. M. & BILIMORIA, E. D. 1977 Heat transfer in rotating cylindrical cavities. *J. Mech. Engng Sci.* **19**, 175.

OWEN, J. M. & ONUR, H. S. 1983 Convective heat transfer in a rotating cylindrical cavity. *Trans. ASME* A: *J. Engng Power* **105**, 265.

OWEN, J. M. & PINCOMBE, J. R. 1980 Velocity measurements inside a rotating cylindrical cavity with a radial outflow of fluid. *J. Fluid Mech.* **99**, 111.

OWEN, J. M. & ROGERS, R. H. 1983 Solution of the integral momentum equations for an Ekman layer in a heated rotating cavity. Part 1: The full equations and the linear approximation. *School of Engng and Appl. Sci., Univ. Sussex, Rep.* TFMRC/15a.

PINCOMBE, J. R., OWEN, J. M. & ROGERS, R. H. 1983 Solution of the integral momentum equations for an Ekman layer in a heated rotating cavity. Part 3. Comparison between theory and experiment. *School of Engng and Appl. Sci., Univ. Sussex, Rep.* TFMRC/17a.

ROGERS, R. H. & OWEN, J. M. 1983 Solution of the integral momentum equations for an Ekman layer in a heated rotating cavity. Part 2. The nondimensional form of the equations and the numerical solutions. *School of Engng and Appl. Sci., Univ. Sussex, Rep.* TFMRC/16a.